Characterization of the Puffing Phenomenon on a Pool Fire

MANDIN P. AND MOST J-M.
Laboratoire de Combustion et de Détonique
Unité Propre de Recherche CNRS n°9028
Université de Poitiers - ENSMA
ENSMA - Site du FUTUROSCOPE
France - 86960 FUTUROSCOPE Cedex

ABSTRACT

Experiments are conducted to study the effect of buoyancy on the pulsation frequency of a diffusion flame stabilized on a horizontal surface. A pool fire is simulated, in a pressure vessel, by injecting a gaseous fuel through a porous flat horizontal burner, air for combustion is introduced at low velocity from below the burner. The flame behavior is investigated at different gravity levels from reduced gravity to centrifuge conditions - 12 times normal gravity (atmospheric pressure) and at ambient pressures ranging from 0.03 MPa to 0.3 MPa (normal gravity). To model the puffing phenomena, Navier Stokes equations are arranged to define a characteristic equation for a gravity wave propagation those celerity is related to flame frequency. This wave propagates horizontally inducing an integer number of nodes n. Its wave length depends on the mode selection and is expressed as the root mean square of gravity. The vertical convection deteriorates the gravity wave, leading to instable flow. The tridimensional gravity wave induces the puffing phenomenon.

KEYWORDS: *pool fire, puffing, buoyancy effects, diffusion flame.*

INTRODUCTION

Many experimental studies have been conducted to describe the structure of a buoyant diffusion flames in an attempt to determined the air entrainment by the fire plume. The main motivation for these studies was to obtain a better definition of the flame geometry and structure [1-4] and to get more information concerning distribution of the heat released by the diffusion flame. The objectives are to define the boundaries of the region in which most of the heat is liberated. Zukoski [5] described the flame structure, by using a technique based on video recordings of natural gas originating from axisymetric porous bed burners. Large structures of flames were observed as a consequence of the flapping motion of the flame

surface close to the burner [1,2,6,7,8]. The flame pulsation induces puffs which play an important role in fixing entrainment, combustion rates and also the flame geometry and the flame radiance. These structures appear to be vortex like rings which form periodically and then rise due to buoyancy. The completion of combustion in these structures at the top of the flame is primarily responsible for the fluctuations in the flame height which are representative of these flames. Flame pulsation frequency [9-11] measurements have been correlated with physical dimension associated with flame surface [12], burner diameter [8,13] for a wide variety gas, liquid and solid fuels. A power law fit to the data yields [13]: $f = 1.5D^{-0.5}$.

More recently, Cetegen [14] developed an experimental study to identify the mechanism responsible for the quasi-periodic oscillations near the source of these flames. He found that:

- helium plumes exhibited puffing with puffing frequencies similar to the flames scaling with $D^{1/2}$;
- the flame front motion near the burner surface is coupled with the downstream development of large scale flaming structures.

Cetegen [14] concluded that puffing is primarily a result of buoyant flow instability of purely fluid mechanical nature. This mechanism involves the strong coupled interaction of a toroidal vortex formed at a short distance above the burner surface. A kinematic analysis, proposed by Cetegen [14] is capable of predicting the frequency - diameter dependence including the effect of source fuel velocity through the Richardson number ($Ri \in [10^1;10^5]$). For high Richardson number ($Ri > 10^4$), the frequency f varies as $f \propto \sqrt{\frac{g}{D}}$.

The present work provides a comprehensive account of experiments conducted that complement the work of Most et al [15] and serves to understand the physical mechanism of puffing by changing the buoyant conditions applied to a diffusion flame. In the following sections, we describe the experimental set-up and the combustion environment corresponding to various theoretical heat release rates, pressure and gravity conditions. A model based on wave theory is developed to formalize the pulsation evolution and properties. Consequently, the flame appears tridimensional, and a number of characteristic structures are defined. This theoretical result is successfully confronted to actual structures observed at the edge of a liquid pool fire.

EXPERIMENTAL SETUP AND DIAGNOSTIC METHODS

In the present study, the horizontal surface burning of a solid polymer is simulated by injecting a gaseous fuel through a porous flat plate. A schematic of the experiment apparatus is presented in Fig. 1. The basic component is a small scale ($6.2\ 10^{-2}$ m diameter), flat surface, porous (sintered bronze), diffusion flame burner that is enclosed in a 0.3 m diameter and 1.0 m height vessel. The gaseous fuel is injected at low velocity (high Richardson number) through the porous burner. Cold ambient air is injected also at low velocity in the lower part of the vessel. Ethane is selected to minimize buoyancy effects of the cold gases (density being close to air). The combustion products are vented 0.3 m under the top of the vessel by a hood such that the vessel pressure is maintained constant during the experiment. The vessel has four pyrex windows to allow flame visualization. The tests presented are conducted with ethane

flames with $\dot{Q} = 1.1$ kW theoretical heat release, corresponding to a Richardson number of 6.10^4 and a Froude number of 6.10^{-5} when calculated at pressure and gravity corresponding to normal earth conditions.

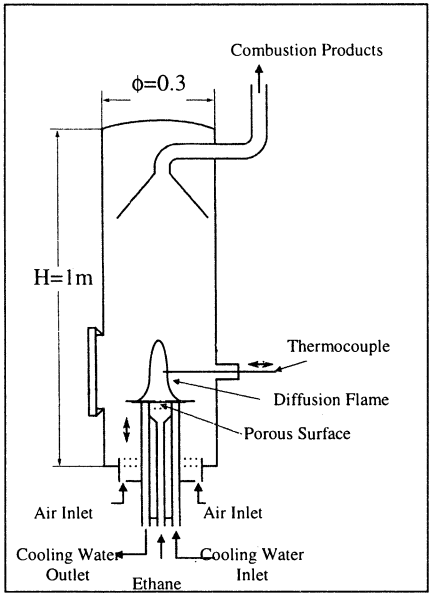

Figure 1. Experimental setup

The tests in high gravity conditions are conducted in a centrifuge facility (radius = 5.5 m). The experimental apparatus (vessel, gas burner, fuel and air supplies and video recorder) are installed aboard the centrifuge basket, the data acquisition and processing system are at the centrifuge axis. Tests are conducted at dimensionless over-gravity conditions g/G included in the 1 to 10 range (g and G are respectively the actual and normal earth gravity acceleration).

The actual local acceleration in the flame is due to earth gravity, entrainment acceleration, and Coriolis acceleration. The flame length being of the order of 0.1m, the entrainment acceleration field is supposed uniform in the direction perpendicular to the burner when g is sufficient ($g \geq 4G$). It has been estimated that a maximum entrainment/Coriolis forces occurs for g =3G [16, 17] with negligible consequences on macroscopic flame properties as length or frequency. In the present work, Coriolis acceleration is assumed to be negligible on the value of the frequency of the periodic phenomenon.

Experiments are also performed in reduced and micro-gravity conditions (0G and 0.2G) in an aircraft following a parabolic trajectory at an ambient pressure P of 0.08 MPa.

Tests are also conducted at normal gravity, for theoretical heat release $\dot{Q}$ and pressure level P varying respectively from 0.5 to 2.0 kW and 0.03 to 0.3 MPa.

Complementary observations are made in laboratory on a liquid pool fire (ethanol, hexane and kerosene) for diameters varying between 0.06 and 0.23 m and on a rectangular porous burner (gaseous fuel: propane; size: 0.15 x 0.25m^2) subject to a forced flow.

Visualizations of the spontaneous flame emission is made by video recording of two cameras oriented toward the flame in two perpendicular directions. The flame being non-stationary. A statistical imaging treatment is performed defining an average and fluctuating luminous flame intensity field. The whole mean temperature field is determined by a 75 10^{-6} m diameter Cr/Al bare wire thermocouple moved by stepping motors in the reactive zone. The oscillation frequency of the flame is obtained either by direct analogue processing of the output signal of a photo detector placed on the video screen, or a spectral processing (Fast Fourier Transformation) of the thermocouple signal.

EXPERIMENTAL RESULTS

At normal gravity, the flame is luminous and presents the well known McCaffrey type characteristic regions (persistent and intermittent flame zones, buoyant plume) [7]. Fluctuating luminous intensity field in the left part of fig. 2, perfectly shows the two extreme puffing positions (maximum of fluctuating luminous intensity). The statistic treatment of video recordings exhibits the area defined by the intermittent location of the luminous flame surface S_f (right side of Fig 2) and its anchoring point at the burner edge. Soot incandescence is non-stationary, and appears for the lower position of S_f. The puffing frequency is 7.1 Hz everywhere in the flame (Fig. 3).

In micro-gravity, a blue flattened flame floats over the burner, and the puffing phenomena disappears. But for a reduced gravity condition (g = 0.2G), the flame becomes luminous with a stable cylindrical shape and puffing reappears with f = 3 Hz. By increasing the gravity level, the flame behavior is modified and becomes non luminous when g > 4G: the flame moves toward the burner, its color changes from yellow to blue, and the flame oscillation frequency f determined in the upper flame zone, increases (Fig. 4). For gravity levels smaller than 8G, the results give a ½ power law dependence of f on g in good agreement with theoretical development and experimental results obtained with diffusion flames [17, 18, 19, 20]. For g < 8G, the Coriolis force not taken into account in the Cetegen model, seems without severe consequences on the frequency value. But for gravity levels g > 8G, the frequency dependence law seems not representative of the experimental flame frequency. The video sweeping rate (25 frames/s) is too low to follow the flame fluctuations, may bias the measurements. The spectral analysis of the thermocouple signal shows, at the same gravity level, a disappearing of puffing frequency. The laminar regime takes a turbulent character. For g greater than 10G, local flame extinction appear at the burner edges leading to blow-off. The monoperiodic flame character disappears. In summary, for $g \in [0.2\,G\,;\,8G]$, the experimental frequency evolution is given by equation (1) :

$$f \propto g^{0.5} \qquad (1)$$

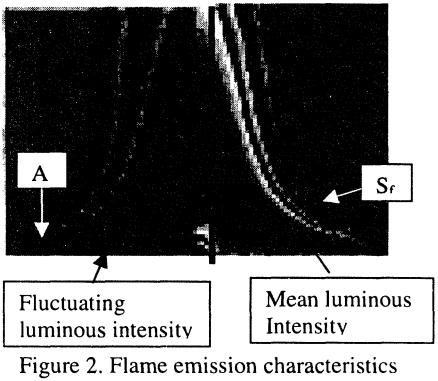

Figure 2. Flame emission characteristics

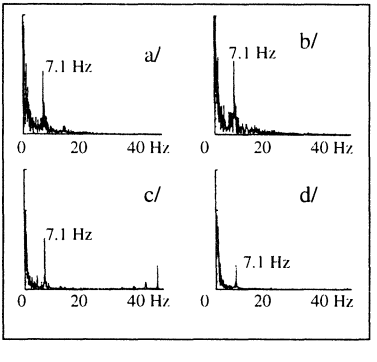

Figure 3.Puffing frequency as a function of the flame location
a/ x/D=0.3; z/D=1.3 b/ x/D=0.15; z/D=1.3
c/ x/D=0.2; z/D=0.2 d/ x/D=0.15; z/D=0.2

The tests made for ambient pressure levels varying from 0.03 MPa to 0.3 MPa, shown that the flame luminous characteristics vary strongly. For P > 0.08 MPa, the flame is yellow, shinny, and small structures appear, wheras the flame oscillation frequency remains constant. For pressure levels decreasing from 0.08 to 0.03MPa, the flame turns blue, the pulsation frequency decreases before becoming steady. The experimental results show that the frequency f obeys the law :

$$\begin{aligned} f &\propto P^{0.22} \quad \text{if} \quad P \leq 0.08 \text{ MPa} \\ f &= 7.1 \text{ Hz} \quad \text{if} \quad P \geq 0.08 \text{ MPa} \end{aligned} \tag{2}$$

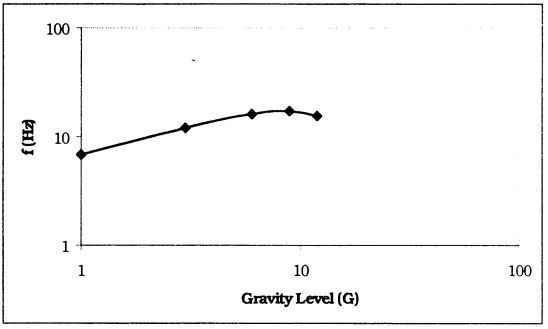

Figure 4. Puffing frequency as a function of gravity

The same trend is obtained with the increase of the theoretical heat release : f increases for 0.5 < $\dot{Q}$ < 1.3kW becoming constant for larger values of $\dot{Q}$, according to the law :

$$\begin{aligned} f &\propto \dot{Q}^{0.1} \quad \text{if} \quad \dot{Q} \leq \dot{Q}^{\circ} = 1.3\text{kW} \\ f &= 7.25\text{Hz} \quad \text{if} \quad \dot{Q} > \dot{Q}^{\circ} \end{aligned} \tag{3}$$

For lower mass flow rates (smaller characteristic lengths), the dispersion of $f \propto D^{-1/2}$ observed [14] is stronger (low Richardson number). In this work, the measured pyrolysis mass flow rate measured for a liquid pool fire (diameter 6 10^{-2} m) and for ethane, hexane, heptane, and octane fuels fire, is greater than the critical value. The corresponding heat release verifies $\dot{Q} \geq \dot{Q}^{0}$ and f appears approximately constant. The good law seems to be $f \propto D_f^{-1/2}$, where the D_f diameter is calculated from the radial anchoring point coordinate, verifying $D_f \cong D$. The larger gap is obtained for smaller diameter values with a small dispersion from the $f \propto D^{-1/2}$ law [14].

PUFFING MODELING

A theoretical model is developed to predict the monoperiodic puffing frequency observed previously in all flames (Fig. 2 & 3). The reactive flow is assumed non-stationary, with negligible viscous effects. A 2D Cartesian coordinate axis system is chosen with origin located at the burner edge and with thenozzle in the x-y plane. A particular mathematical surface S_f (Fig 2 right) is used and defined as the maximum temperature location. S_f is anchored at the point A_f on the burner edge (Fig. 2 left). The model consists of describing the intermittent displacement of S_f as Lagrangian in the aerothermochemical flame field. Displacements are

supposed to be small around the average location of S_f, written $\overline{S_f}$. For each point M_f chosen on S_f, it is assumed that:

- the fluctuations of temperature, density, and chemical reactants around their average values (intermittent motion of S_f) are negligible. Then $\overline{\text{grad}(T)} = 0$ on S_f for zones where Temperature is constant which is true near the absolute maximum temperature in the flame (burner edge);
- instantaneous velocity vector $\vec{V}$ on S_f is the sum of time averaged $\overline{\vec{V}}$ and fluctuating $\vec{V}'$ velocity vectors, due to the S_f displacement, $\vec{V} = \overline{\vec{V}} + \vec{V}'$.

This last hypothesis is necessary because it appears that the S_f displacement (i.e. puffing phenomenon) can be attributed to intermittent air entrainment in the flame [20]. Previous works and ours show that puffing and convective characteristic times are of the same order of magnitude, revealing their coupling. Then, we assume that the displacement of S_f is the response of unsteady flow of air.

Definitions : Each point $M_f(x_f, y_f, z_f) \in S_f$ fluctuates around the location of the mean point $\overline{M}_f(\overline{x}_f, \overline{y}_f \overline{z}_f)$, the time dependent displacement $\vec{D}(X,Y,Z)$ is:

$$\vec{D}(t) = \begin{cases} X = x_f - \overline{x}_f \\ Y = y_f - \overline{y}_f \\ Z = z_f - \overline{z}_f \end{cases} \qquad (4) \qquad \text{and} \qquad \vec{V}' = \frac{\partial \vec{D}}{\partial t} \quad \Rightarrow \quad \frac{\partial \vec{V}'}{\partial t} = \frac{\partial^2 \vec{D}}{\partial t^2} \qquad (5)$$

Mass conservation : An elementary average flame volume V is defined in Fig. 5 $(dx, dy, \overline{z}_f)$, with a mass equal to $m(t) = \int_x^{x+dx} \int_y^{y+dy} \int_0^{\overline{z}_f} \rho \, dxdydz$. At t+dt, after neglecting the second order terms, the mass m(t) becomes:

$$m(t+dt) = \int_x^{x+dx+dX} \int_y^{y+dy+dY} \int_0^{\overline{z}_f+Z} \rho dxdydz \cong \int_{z=0}^{\overline{z}_f} \rho dzdxdy + \int_{z=0}^{\overline{z}_f} \rho dzdxdY + \int_{z=0}^{\overline{z}_f} \rho dzdXdy + \rho_f Zdxdy \quad (6)$$

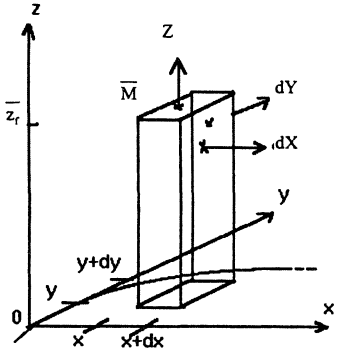

Figure 5. Mathematical domain and displacement considered in the model

During the S_f displacement, the mass of V is assumed conserved [m(t)=m(t+dt)], then the displacement Z is then obtained as:

$$Z = -\frac{1}{\rho_f}\int_{z=0}^{\bar{z}_l} \rho\, dz \left(\frac{\partial X}{\partial x} + \frac{\partial Y}{\partial y}\right) = -\frac{1}{\rho_f}\int_{z=0}^{\bar{z}_l} \rho\, dz\, div(\vec{D}_H) \qquad (7) \qquad \text{with} \quad \vec{D}_H = \begin{pmatrix} X \\ Y \\ 0 \end{pmatrix} \text{ from (4).}$$

Momentum conservation on S_f : For the studied diffusion flames (low Froude numbers), with velocities respecting the criterion M< 0.3 (M = Mach number), the pressure field can then be considered unmodified because the flame flow (barometric distribution) for our study is in the low frequency region, then

$$\frac{\partial \vec{V}}{\partial t} + \overline{\overline{grad}}(\vec{V})\,\vec{V} = -\rho_f \vec{g} - \overline{grad}(P) = -\frac{\rho_f - \rho_\infty}{\rho_f}\overline{grad}(g\,z) \qquad (8)$$

By introducing the $\vec{V}$ decomposition in Eq. (8), and supposing the two conservation terms not coupled, we obtain :

$$\underbrace{\frac{\partial \vec{V}'}{\partial t}}_{I} + \underbrace{\overline{\overline{grad}}(\vec{\bar{V}})\,\vec{V}'}_{II} + \underbrace{\overline{\overline{grad}}(\vec{V}')\,\vec{\bar{V}}'}_{III} + \underbrace{\overline{\overline{grad}}(\vec{V}')\,\vec{\bar{V}}}_{IV} = \underbrace{-\frac{\rho_f - \rho_\infty}{\rho_f} g\,\overline{grad}(Z)}_{V} \qquad (9)$$

The sum II + III, representing the convection of the motion by the velocity fluctuation, is neglected. IV is also neglected for small values of $\vec{\bar{V}}$ (convection of the fluctuating motion), the validity of this assumption will be discussed later. Then, Eq. (9) becomes:

$$\frac{\partial \vec{V}'}{\partial t} = \frac{\partial^2 \vec{D}}{\partial t^2} = -\frac{\rho_f - \rho_\infty}{\rho_f} g\,\overline{grad}(Z) \qquad (10)$$

Wave propagation equation :

$\frac{\partial^2 \vec{D}_H}{\partial t^2}$ in Eq. (10) is obtained by twice differentiating z (equation (7)) with respect to time, which results in:

$$\frac{\partial^2 Z}{\partial t^2} = \frac{\rho_f - \rho_\infty}{\rho^2_f}\int_{z=0}^{\bar{z}_l} \rho\, dz\; g\,\Delta_H Z + \frac{1}{\rho_f}\int_{z=0}^{\bar{z}_l} \rho dz\, g\,\overline{grad}\left(\frac{\rho_f - \rho_\infty}{\rho_f}\right)\overline{grad}(Z) \qquad (11)$$

For $\overline{M}_f(\bar{x}_f, \bar{y}_f, \bar{z}_l) \in \overline{S_f}$; $\overline{grad}(T) \approx \vec{0}$ then $\overline{grad}\left(\frac{\rho_f - \rho_\infty}{\rho_f}\right) \approx \vec{0}$, Eq. (11) is reduced to a characteristic equation of the gravity wave propagation (Δ_H is the Horizontal Laplacian operator):

$$\frac{\partial^2 Z}{\partial t^2} - c(\bar{z}_f)^2\, \Delta_H Z = 0 \qquad (12)$$

where wave speed :

$$c(\bar{z}_f) = \left(-\frac{\rho_f - \rho_\infty}{\rho_f}\int_{z=0}^{\bar{z}_l} \rho dz\, g\right)^{1/2} = \lambda(\bar{z}_f)\, f(\bar{z}_f) \qquad (13)$$

As shown in Figure 3, the frequency f is constant in the entire flame during the propagation of the wave along the S_f region, which respects our hypothesis. Therefore, the wave length λ and the velocity c vary as the root mean square of gravity and are functions of $\bar{z}_f$.

DISCUSSION OF THE THEORETICAL MODEL

The model hypothesis are best verified when the considered point M_f is closest to the burner edge. Experimentally, this mathematically defined zone is also of particular interest: M_f birth place of the S_f displacement area, and of the luminous flame character (radical species blue color lost), and it defines an inflection curvature on S_f.

Horizontal Gravity Wave Propagation

In the orthoradial direction y, on the axisymetric-supposed $\overline{S_f}$ surface, concentric circles centered on the pool axis can be defined. In this direction, convection is rigorously nul (lower values for $\bar{V}$ and $\overline{\overline{grad}}(\bar{V})$), and each point on those circles, which verifies $\overline{z_f}$ = cste, defines a constant celerity c. Then, according to Eq. (12), each point generates a wave which propagates in the horizontal and orthoradial directions, and interferes with neighbors. In those conditions the wavelength should satisfy the general stationary wave condition :

$$n\lambda(\overline{z}_f) \cong 2\pi D_f \qquad \text{with} \quad n \in N^* \qquad (14)$$

For other wavelength the interference is not constructive, and the wave is not amplified . D_f is the circle diameter considered on S_f. Relation (14) is verified near the burner edge where $D_f \cong D$. A particular celerity c_f, wavelength λ_f, and tridimensional structure number n on S_f, are defined (Fig. 6) and assumed to be conserved in the whole flame (Eqs. 13 & 14) :

$$c_f = \left(-\frac{\rho_f - \rho_\infty}{\rho_f^2} \int_{z=0}^{\bar{z}_f} \rho dz g \right)^{1/2} = \lambda_f f = \frac{2\pi D}{n} f \qquad (15)$$

Equation (14) defines an infinite number of modes, each characterized by n. For a given diameter D, the experimental frequency value f is fixed [14], as far as other relevant parameters are kept constant. Then, the flame selects one mode among an infinity of possibilities. This theoretical finding is confirmed by the tridimensional luminous structures observation both under Pyrex pool fires (Fig. 7) and over a rectangular porous burner. In this case, equation (14) is written $n\lambda(\overline{z}_f) \cong 2\pi L$, the waves propagate along the symmetrical direction, interfering with reflected waves at the surface edge. It appears that the importance of the convection applied on S_f is an important parameter for the mode selection. For large values of n, the tridimensional character of S_f is amplified by its size and the local chemical rate. A lower n value reduces the aerodynamical stress on S_f, which are in competition with superficial capillary surface effects. Then n should appears as an optimization of this compromise.

The Vertical Wave Convection

The theoretical model neglects the convective transport of the fluctuation flow $\overline{\overline{Grad}}(\bar{V})\bar{V}' + \overline{\overline{Grad}}(\bar{V}')\bar{V}$. This assumption is valid in the orthoradial direction due to nil convective transfer (no swirl), only an attenuation of the displacement amplitude can appear, while the wave length and frequency are not affected.

As we observe for g>8G, the assumption that a small mean velocity gradient exists close to the flame(air entrainment and turbulence) breaking the $g^{1/2}$ dependency.

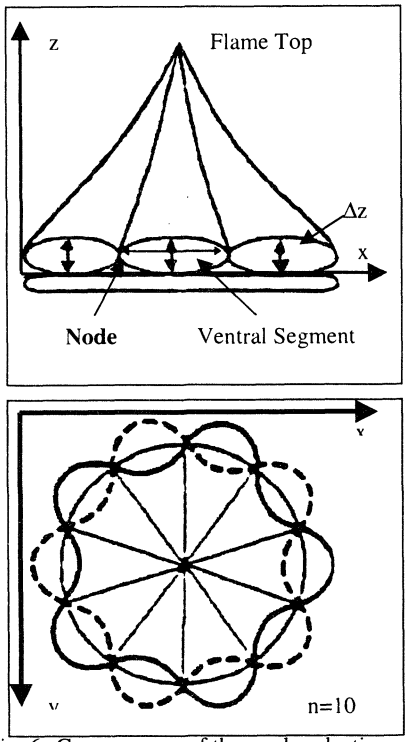

Fig. 6. Consequence of the mode selection in (x,z) and (x,y) planes

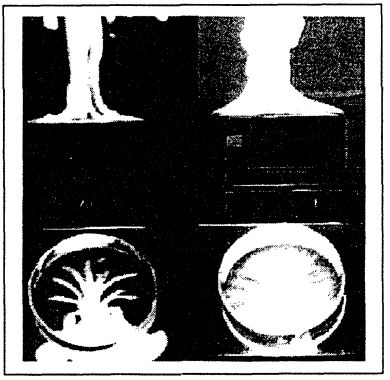

Fig. 7. Luminous tridimensional structures seen under ethanol (left) and hexane (right) pool fires (D=0.23 m).

The wave generated near the burner is convected from S_f to the flame top (macroscopic visible puffing phenomenon). In this curvilinear direction, the wave information (S_f deformation) is convected by the flow to the top of the flame inducing the intermittent extinction and luminous structure creation. The intermittent McCaffrey flame zone is then defined as the region where radial deformation of S_f, due to the puffing wave, is of same order of S_f radius. The interference of waves born over the burner edge, results in S_f surface tear. The length induced by this phenomenon can be related to the convection with a characteristic time f^{-1} and a mean flow vertical velocity $L_f \propto \int_0^{f^{-1}} \overline{\vec{V}_f}\, \vec{z}\, dt$. $\overline{\vec{V}_f}$ is the mean velocity of puff during its path from the burner edge to the flame top.

Puffing Consequences for Flame Properties

Temperature in the flame presents a monoperiodic time evolution (Fig. 3) which can be written by assuming negligible a non-fundamental frequency participation :

$$T(t) = \overline{T} + \Delta T \mathrm{Sin}(2\pi f\, t + \varphi) \qquad (16)$$

The fluctuation amplitude ΔT can experimentally reach 25% of the time averaged temperature $\overline{T}$. Here, ΔT is supposed proportional to RMS measured temperature, such as $\Delta T = \sqrt{2}\sqrt{\overline{T'^2}}$.

(thermocouple time constant and measurement duration are chosen in accord with the fluctuation characteristic time f^{-1}).

The average radiative heat transfer properties calculations need the knowledge of the $\overline{T^4}$ quantity, which is, obtained from equation (16) :

$$\overline{T^4} = \overline{T}^4\left[1+3\left(\frac{\Delta T}{\overline{T}}\right)^2+\frac{3}{8}\left(\frac{\Delta T}{\overline{T}}\right)^4\right] \qquad (17)$$

Then, the unsteady flame character increases the radiative heat transfer. The same conclusion was obtained by Grosshandler [21] for many mathematical time functions of temperature (squared, serrated, sinusoidal).

The unsteady flame is also tridimensional (Fig. 7) and the folding of S_f are described by equation (18) :

$$z_f\left(r\equiv\frac{D}{2};y,t\right)=\overline{z_f}+\Delta z\,\mathrm{Cos}\left(\frac{n}{D}y\right).\mathrm{Sin}\left(2\pi f t\right) \qquad (18)$$

where $\Delta z = |Z|$, according with model notations, and y is the orthoradial coordinate. From (18) the scale of the anisotropic gravity turbulence can be predicted and a better estimation for the plume turbulence can be obtained. This last result is very important: the length scale (generally the diameter) can change by an order of magnitude if n = 10.

Tridimensional Puffing Flame Evolution with Combustion Parameters

Equation (15) can be rewritten as :

$$f=\frac{n}{2\pi\sqrt{D}}\left(-\frac{\rho_f-\rho_\infty}{\rho_f^2}\int_{z=0}^{\overline{z}_f}\rho\,dz\frac{g}{D}\right)^{1/2} \qquad (19)$$

which have to be compared with the well known frequency law evolution $f\propto\left[\frac{g}{D}\right]^{\frac{1}{2}}$. The consequence on tridimensional flame character is given in relation (20) :

$$n=\frac{2\pi\sqrt{D}}{\left(-\frac{\rho_f-\rho_\infty}{\rho_f^2}\int_{z=0}^{\overline{z}_f}\rho\,dz\right)^{1/2}} \qquad (20)$$

For pool fires, frequency verifies $f\propto D^{-1/2}$ evolution law [14]. In this case, the tridimensional flame character also varies. The denominator in equation (20) can be supposed constant, so the flame pleats should follow the law : $n\propto\sqrt{D}$. This observation has been experimentally demonstrated for ethanol pool fire. For pool fires, the frequency is weakly dependent of the fuel chemical nature [14]; but, tests done with more sooty fuels (hexane, heptane, octane), show a great difference in the tridimensional character (Fig. 7): n becomes linear with D ($n\propto D$) for the same diameter range. In those flames, the average flame temperature is lower than in ethanol flame, that could explain the increase of n simultaneously to the increase of the radiative energy fraction χ_r. The selection of the mode is changed by the elastic property modification of the S_f surface due to the presence of soot. This result confirms the coupling between aerodynamic and surface S_f properties. Some tests in a bidimensional Cartesian pool fire with cross flow show an increase of n both with the aerodynamic stress ($n\propto V^{0.3}$) and

with an increase of the initial fuel velocity V_0, whereas the frequency f keeps almost constant (equation (3)). Then, the aerodynamic stress on S_f appears to be important in the determination of the flame mode. The gravity level g does not explicitly appear in relation (20) but affects the mode choice through the induced air entrainment and aerodynamic stress. In macrogravity condition, V increases with S_f and model assumptions concerning the velocity, remain valid. Particularly, for g greater than 8G, it appears that the flow arround S_f becomes more and more turbulent.

CONCLUSION

An original experimental study has been conducted in order to identify the puffing phenomenon in various buoyancy conditions by changing ambient pressure and gravity level. The obtained experimental results on flame frequency oscillation are used to develop a new theoretical model for puffing using the assumption of a Lagrangian flame sheet displacement and the mechanical wave propagation theory. It is shown that the wave is born close to the burner and propagates in the orthoradial horizontal direction whereas it is convected by gravity in the ascendant direction. The perturbation, convected at the flame top, induces the puff in the intermittent McCaffrey zone. The orthoradial propagation induces a tridimensional character to the flame, which is experimentally confirmed (Fig. 7).

Then, the puffing phenomenon is attributed to gravity which induces thermal (unstable equilibrium due to cold air above hot products layer) and dynamic (aerodynamic stress gradient) instabilities. These gravity effects seem to be confirmed by the puffing phenomenon disappearance in micro-gravity conditions. The luminous flame character disappears through the soot formation evolution. On earth, it appears that the sooty zone is tridimensional (Fig. 7) and unsteady and becomes important when S_f is in its lower position during the puffing cycle. The main chemistry regime on S_f is time dependent because of the intermittent displacement. The puffing phenomenon then appears as a self-sustained relaxation oscillation due to the alternative air entrainment in the flame [20].

ACKNOWLEDGMENTS

The authors gratefully acknowledge Mrs. D. Durox, P. Joulain, J. Torero and C A. and Fernandez Pello for their scientific regards. This study was supported by CNRS, MESR, CNES, ESA, LCPC.

NOMENCLATURE

c	Celerity	($m.s^{-1}$)	L	Length	(m)
D	Diameter	(m)	m	Volume mass	(kg)
$\vec{D}$	S_f displacement	(m)	M	Mach number	
div	Divergence	(m^{-1})	n	Stationary structures number	
f	Frequency	(Hz)	P	Pressure	(MPa)
grad	Gradient	(m^{-1})	$\dot{Q}$	Theoretical heat	(kW)
g	Acceleration	($m.s^{-2}$)	r	Radial coordinate	(m)
G	Earth gravity = 9.81 $m.s^{-2}$		Ri	Richarson number	

t	Time	(s)
T	Temperature	(K)
$\overline{T}$	Mean temperature	(K)
T'	Fluctuating temp.	(K)
ΔT	Temperature ampl.	(K)
$\vec{V}$	Velocity	($m.s^{-1}$)
$\overline{\vec{V}}$	Mean velocity	($m.s^{-1}$)
$\vec{V}$ '	Fluctuating velocity	($m.s^{-1}$)
x, y, z	Coordinates	(m)
x_f, y_f, z_f	M_f coordinates	(m)
$\overline{x}_f, \overline{y}_f, \overline{z}_f$	Mean $\overline{M}$ coordinates	(m)
X, Y, Z	M_f displacement	(m)
Δz	Vertical displ.	(m)

Subscripts

f	Flame properties
H	Horizontal
∞	Ambient properties

Greek letters

Δ_H	Laplacian operator	(m^{-2})
λ	Wave length	(m)
ρ	Density	($kg.m^{-3}$)
φ	Phase of a signal	(rad)
χ_r	Radiative energy fraction	

REFERENCES

1. Rasbash D. J., Rogowski Z. W., and Stark, G. W. V., *Fuel*, 35, 94, (1956)
2. Thomas P. H., *9th Symp. (Int.) on Combustion*. The Comb. Inst., 1963, p 844
3. Steward F. R., *Comb. Sc. & Technology*, 2, 203, (1970)
4. Heskestad G., *18th Symp. (Int.) on Combustion*. The Comb. Inst., 1981, p 951
5. Zukoski E. E., *20th Symp. (Int.) on Combustion*. The Comb. Inst., 1984, pp 361-366
6. Cox G., and Chitty R., *Combustion and Flame*, 39, 191-209, (1980)
7. McCaffrey B.J., Nbsir, 79-1910, NBS, Dpt of Commerce, Washington DC. (1979)
8. Weckman E.J. and Sobiesiak A., *22sd Symp.(Int.) on Comb.* The Comb. Inst.,1988,p 1299
9. Byram G. M. and Nelson R. M., *Fire Technology*, 6, 102, (1970)
10. Schonbucher, A., Arnold, B., Banhardt, K., Bieller, V., Kasper, H., Kaufmann, M., Lucas, R., and Schiess, N.: *21st Symp. (Int.) on Combustion*. The Comb. Inst., 1987, p 83
11. Hamins A., Yang J. C., and Kashiwagi T., *24th Symposium (Int.) on Combustion*. The Combustion Institute, 1992, pp 1695-1702
12. Beyler, C., L.: *Fire Safety Journal*, 11, 53, (1986)
13. Pagni, P. J.: *Applied Mechanics Reviews*, p166 (1990)
14. Cetegen, B. M. and Ahmed, T., A.: *Combustion and Flame*, 93, pp157-184, 1993
15. J-M. Most, P. Mandin, J. Chen, P. Joulain, D. Durox, A. C. Fernadez Pello, *26th Symp. Int on Comb.*, , pp1311-1317, (1997)
16 Yuan, T., Durox, D., Villermaux E.: *Exp. in Fluids*, 17, pp337-349, 1994
17 Durox, D., Yuan N, T., Baillot, F., Most, J-M.: *Comb. and Flame*, 102, pp501-511, (1995)
18. Baum H.R. and McCaffrey B.J, Proceedings, *2nd Symp. of Fire Saf. Sc.*, 129, 1989
19. Bejan, A.: *Journal of Heat Tranfer*, 113, pp261-263, (1991)
20. Zhou, X.C. and Gore, J.P., *20th Symposium (Int.) on Combustion*, The Combustion Institute, 1995, pp361-366
21. Grosshandler, W.L., and Joulain, P., 10th ICDERS, August 1985, (1986)